Progress In Electromagnetics Research C, Vol. 106, 89–103, 2020

Modeling and Experimental Analysis of Three-Dimensional Crossed Coil Structure for Misaligned Wireless Power Transfer System

Jiaxiang Song[1, 2, *], Huilin An[1, 2, *], Yanhong Li[1], Chao Zhang[1], and Guoqiang Liu[1, 2]

Abstract—The coaxiality of the transmitter and receiver has a significant impact on the efficiency in a wireless power transfer system. In order to keep high system efficiency, a novel coil structure is studied in this paper. Several plane coils are crossed to make up a three-dimensional coil structure in the transmitter, which will make sure the system in the state of strong magnetic field coupling. In the theory part, the magnetic field equation of different relationships between transmitter and receiver is deducted in detail. In the simulation part, the performance of the three-dimensional coil structure has been studied. The simulation results show that the new coil structure can generate a rotating magnetic field, and the rotating magnetic field will keep the system in the state of the strong magnetic field coupling in the simulation model. In the experimental part, the three-dimensional coil structure has been compared to a plane coil structure. The experimental results show that the efficiency of the three-dimensional coil structure is increased above 10% in the misalignment situation. The simulated and experimental results show that the new three-dimensional coil structure has a better performance in the misalignment situation than the plane coil structure in a wireless power transfer system.

1. INTRODUCTION

In the past few years, wireless power transfer (WPT) has drawn much attention, due to WPT's convenience, simplicity, and non-radiation [1, 2]. As the coaxiality of the transmitter and receiver have a significant impact on the efficiency in the wireless power transfer system, there are many researches on misaligned WPT systems [3–5]. In order to improve the performance of a misaligned WPT system, new coil structures have been designed [6–9]. In [8], three-dimensional transmitter and receiver have been designed, and a 3D coil structure can improve the efficiency of the system obviously. However, the 3D coil structure receiver may be not suitable for some general electric devices, such as cell phone and small robots, and plane coil structure receiver is more suitable for these applications. In [9], a 3D structure transmitter has been designed, and the receiver is a plane coil structure. Their system efficiency can reach 90.2%; however, the transmitter in [9] is spherical, which may need an additional support structure in the practice application. In order to increase the distance of the misaligned WPT system, a repeating coil has been used in the system [10, 11]; however, the repeats cannot be applied in some situation. The magnetic field shaping technique is also used in [12], but there are three independent power supplies in their system, which increases system complexity. In order to increase the efficiency, low loss materials have also been tried to apply in the system [13–15]; however, the price of low loss materials should not be ignored.

In this paper, compared to [8], we use a plane coil structure for the receiver to improve system applicability. Comparing [9] to our paper, a cuboid is studied in our paper. The system efficiency is reduced to 86.7%, but the system may omit additional support structure. Comparing [10, 11],

Received 24 May 2020, Accepted 31 August 2020, Scheduled 13 October 2020

* Corresponding author: Jiaxiang Song (songjiaxiang@mail.iee.ac.cn).

[1] Institute of Electrical Engineering, Chinese Academy of Sciences, Haidian District, Beijing, China. [2] School of Electronic Electrical and Communication Engineering, University of Chinese Academy of Sciences, Haidian District, Beijing, China.

the magnetic field shaping technique is used for the system to overcome the lack of using repeater. Comparing [12] to our paper, there is only one power supplies in our system. Moreover, in this paper, the magnetic field equation of different relationships between transmitter and receiver is deducted in theory part. The verified simulation and experiment are also done.

The rest of the paper is organized as follows. In Section 2, the basic theory of a 3D crossed coil structure applied in a misaligned WPT system is explained. In Section 3, the mathematical model of the 3D cross coil structure is deducted. In Section 4, the simulation model of the 3D crossed coil is built. In Section 5, the verification experiment is done, and the experimental results are compared with simulation ones. Finally, conclusions are drawn in Section 6.

2. 3D CROSS COIL STRUCTURE FOR WPT SYSTEM

2.1. Traditional WPT System with Magnetic Coupling

Figure 1 shows a block diagram of a general magnetic resonant coupling WPT system. The transmitter side is composed of an AC-DC rectifier, a DC-DC converter, and a DC-AC inverter. The transmitter and receiver are isolated by an air gap, based on the magnetic field shaping technique, and the transmitter can generate magnetic field in different directions, which will couple the receiver for reaching high efficiency transmission.

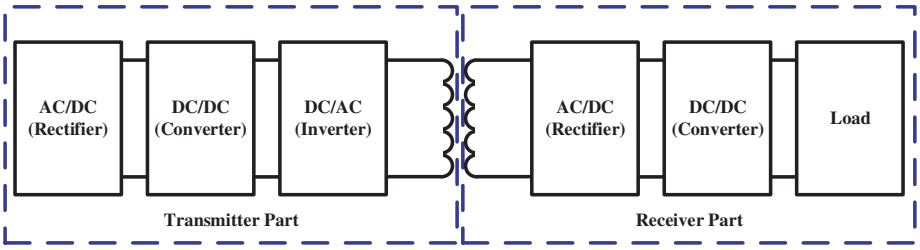

Figure 1. Diagram of a tridtional magnetic resonant coupling WPT system.

2.2. 3D Cross Coil Structure for a WPT System

In Fig. 2, the transmitter coil is composed of several coils with different space angles, and the receiver is a plane coil. The 3D crossed structure transmitter can generate circular rotating magnetic field, and the controller of system will choose the coil of transmitter to make the maximum mutual inductance between one or several coils in transmitter and receiver during the system working time.

It is worth noting that the transmitter has a variety of ways to generate circular rotating magnetic field, such as phase-shift techniques [16, 17]. As for phase-shift techniques, several power supplies load different phase currents in different transmitter coils, and the magnetic field directions can be

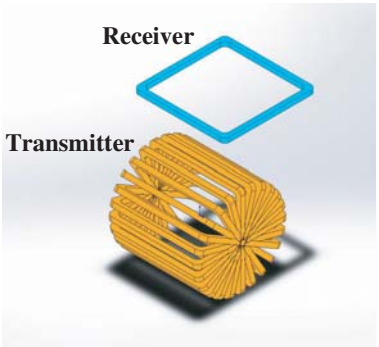

Figure 2. The diagram of 3D crossed coil applied in WPT system in this thesis.

controlled by adjusting the phase of the current. However, several power supplies will increase the system complexity. There is another way to generate circular rotating magnetic field. Because transmitter coils are in different directions, every transmitter coil will generate a magnetic field direction. All the directions of magnetic field generated by transmitter will form a circular rotating magnetic field. The second way of generating circular rotating magnetic field will be used in this paper.

3. THE MATHEMATICAL MODEL OF 3D CROSSED COIL STRUCTURE

Because only one coil of transmitter is power-on, we can simplify the WPT system to a two-coil system. Choosing the space angle of transmitter coil can get maximum mutual inductance between transmitter and receiver.

3.1. Circuit Analysis of Two-Coil WPT System

The equivalent circuit model of a two-coil WPT system shown in Fig. 3(a) can be converted to the T-type model, as shown in Fig. 3(b) [18, 19]. The circuit input and output currents are expressed in the matrix form in Eq. (1) where r_1, r_2, L_1, L_2, C_{S1}, and C_{S2} represent the parasitic resistances, self-inductances, and compensating capacitances of the transmitter and receiver units, respectively. In addition, M is the mutual inductance between transmitter and receiver.

$$\begin{bmatrix} I_1 \\ I_2 \end{bmatrix} = \frac{1}{Z_{\text{det}}} \begin{bmatrix} Z_2 + Z_L & -j\omega M \\ -j\omega M & Z_P + Z_1 \end{bmatrix} \begin{bmatrix} V_{S1} \\ 0 \end{bmatrix} \tag{1}$$

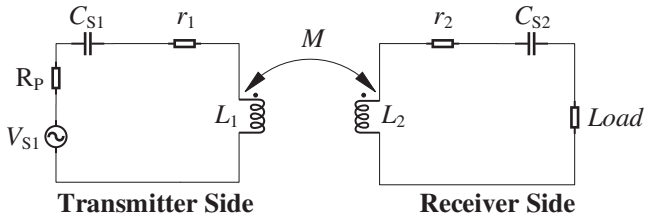

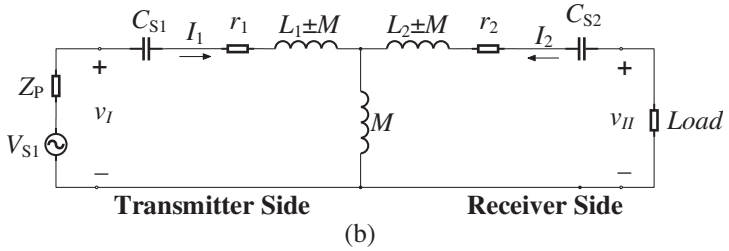

Figure 3. The cross-sectional view of planar coils using for wireless power transfer.

The impedances in Eq. (1) can be expressed as $Z_1 = r_1 + j\omega L_1 + \frac{1}{j\omega C_{S1}}$, $Z_2 = r_2 + j\omega L_2 + \frac{1}{j\omega C_{S2}}$, and $Z_{\text{det}} = (Z_P + Z_1)(Z_2 + Z_L) + \omega^2 M^2$. To simplify the analysis, the transmitter and receiver units are assumed symmetric, i.e., $L_1 = L_2$, $C_{S1} = C_{S2}$, and the resonant frequency can be calculated as $\omega_0^2 = \frac{1}{L_1 C_{P1}} = \frac{1}{L_2 C_{P2}}$. Additionally, source impedance Z_P and load impedance Z_L are assumed purely resistive; $Z_P = R_P$, $Z_L = R_L$. The efficiency is defined as the ratio of the load power to the total input power as in Eq. (2)

$$\eta = \frac{\omega_0^2 M^2 R_L}{(R_P + r_1)(R_L + r_2)^2 + \omega_0^2 M^2 (R_L + r_2)} \tag{2}$$

where $R_{lump} = 2R_L R_P r_2 + r_2^2 R_P + R_L^2 r_1 + 2R_L r_1 r_2 + r_1 r_2^2$.

In Eq. (2), efficiency can be increased through the controlling mutual inductance M between transmitter and receiver. The parasitic resistances r_1 and r_2 should be minimized.

In the resonance status, the receiving power P_L is defined as in Eq. (3).

$$P_L = I_2^2 R_L = \frac{\omega_0^2 M^2 V_{S1}^2}{\left((R_P + r_1)(R_L + r_2) + \omega_0^2 M^2\right)^2} R_L \tag{3}$$

As can be seen in Eq. (3), the receiving power can also be improved through increasing the mutual inductance M between transmitter and receiver. The parasitic resistances r_1 and r_2 should be minimized.

3.2. Analysis Transmitting State between Transmitter and Receiver

When magnetic field is generated in transmitter where the coupling effect occurs effectively, the transfer efficiency and transfer power will be highly likely to decrease, significantly [20, 21]. Because only one transmitter coil is power-on in the WPT system with 3D cross coil structure, the coupling among transmitter is low, which will help the system work on a better performance.

The controller finds that the transmitter coil marked X has the maximum mutual inductance with receiver. The transmitting coil X and receiver are shown in Fig. 4. In Fig. 4, the self-inductances of the transmitter coil X and receiver are L_1 and L_2, respectively. As shown in Fig. 4, transmitter coil X and receiver are crossed with an angle $\theta(0 \leq \theta \leq \pi)$. The size of transmitter coil X is $2a \times 2a$, while receiver is $2b \times 2b$. Based on Neumann's formula [22, 23], the mutual inductance of transmitter coil X and receiver can be written as follows:

$$M = \frac{\mu_0}{4\pi} \oint \oint \frac{\overline{dl_1 dl_2}}{d_{12}} \tag{4}$$

In Fig. 4, conductor A is parallel to conductor E. Conductors A, B, C, and D are on the same plane, and conductors E, F, G, and H also are on the same plane. The plane including conductors E, F, G, and H is parallel to xy-plane. Three cases of coil configurations between transmitter coil and receiver are shown in Fig. 5. The first case [as seen in Fig. 5(a)] is two conductors placed in parallel at a distance d. In Fig. 4, a total of four examples (conductors A and E, conductors C and G, conductors A and G, and conductors C and E) can be observed for this case. The second case [as seen in Fig. 5(b)] is two conductors placed with an angle θ on different planes. In Fig. 4, four examples (conductors B and H, conductors D and F, conductors B and F, and conductors D and H) can be identified as the following second case. Finally, Fig. 5(c) shows the third case, where non-coplanar conductors are apart from each plane. Conductors A and F, conductors A and H, conductors C and F, conductors C and H, conductors E and D, conductors E and B, conductors G and D, and conductors G and B can be considered to

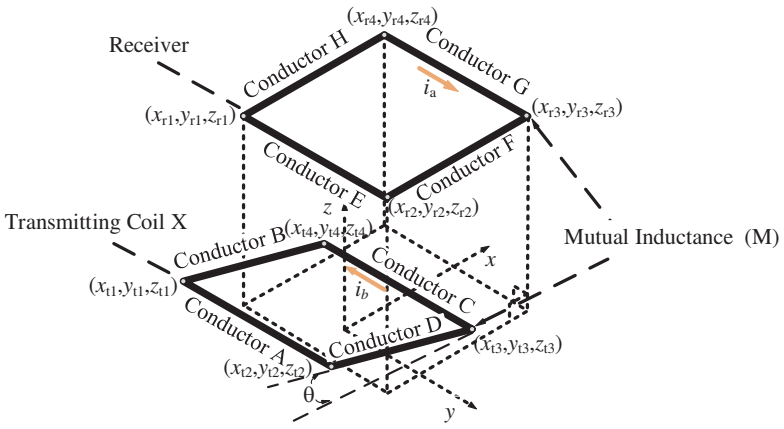

Figure 4. The basic cell ABCD related to the turn-to-turn capacitance.

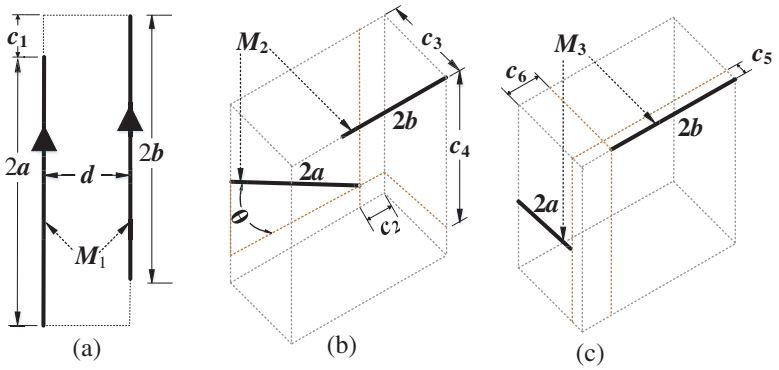

Figure 5. Three cases of wire configurations between transmitter and receiver.

fall under this case. Please note that the mutual inductances of the two perpendicular conductors is always zero [14]. Therefore, the cases of conductors A and F, conductors A and H, conductors C and F, conductors C and H, conductors E and D, conductors E and B, conductors G and D, and conductors G and B are not considered, and their mutual inductances are zero.

The mutual inductance in the first case will be referred as M_1. Based on Eq. (4), M_1 can be calculated as in following equation:

$$M_1 = \frac{\mu_0}{4\pi} \int_{c_1}^{2a+c_1} \int_0^{2b} \frac{dy_t dy_r}{\sqrt{d^2 + (y_t - y_r)^2}} \tag{5}$$

Here, $y_t \in (c_1, 2a + c_1)$, $y_r \in (0, 2b)$.

The mutual inductance in the second case will be referred as M_2. Based on Eq. (4), M_2 can be calculated as in following equation:

$$M_2 = \frac{\mu_0}{4\pi} \int_0^{2b} \int_{c_2}^{c_2+2a\cos\theta} \int_{c_4-2a\sin\theta}^{c_4} \frac{dx_r dx_t dz_t}{\sqrt{(x_r - x_t)^2 + z_t^2 + c_3^2}} \tag{6}$$

Here, $x_r \in (0, 2b)$, $x_t \in (c_2, c_2 + 2a\cos\theta)$, $z_t \in (c_4 - 2a\sin\theta, c_4)$.

The mutual inductance in the third case will be referred as M_3. Because the two conductors are perpendicular, the value of M_3 is zero.

In Fig. 3, combining Eq. (5) and Eq. (6), the mutual inductance between conductors is

$$M_{AE} = M_{CG} = \frac{\mu_0}{4\pi} \int_{y_{t1}}^{y_{t2}} \int_0^{y_{r1}} \frac{dy_t dy_r}{\sqrt{d_{AE}^2 + (y_t - y_r)^2}} \tag{7}$$

Here, $y_t \in (y_{t1}, y_{t2})$, $y_r \in (y_{r1}, y_{r2})$.

$$M_{AG} = M_{CE} = \frac{\mu_0}{4\pi} \int_{y_{t1}}^{y_{t2}} \int_{y_{r4}}^{y_{r3}} \frac{dy_t dy_r}{\sqrt{d_{AG}^2 + (y_t - y_r)^2}} \tag{8}$$

Here, $y_t \in (y_{t1}, y_{t2})$, $y_r \in (y_{r4}, y_{r3})$.

$$M_{BH} = M_{DF} = \frac{\mu_0}{4\pi} \int_{x_{r1}}^{x_{r4}} \int_{x_{t1}}^{x_{t4}} \int_{z_{t4}}^{z_{t1}} \frac{dx_r dx_t dz_t}{\sqrt{(x_r - x_t)^2 + z_t^2 + (y_{r1} - y_{t1})^2}} \tag{9}$$

Here, $x_r \in (x_{r1}, x_{r4})$, $x_t \in (x_{t1}, x_{t4})$, $z_t \in (z_{t4}, z_{t1})$.

$$M_{BF} = M_{DH} = \frac{\mu_0}{4\pi} \int_{x_{r1}}^{x_{r4}} \int_{x_{t1}}^{x_{t4}} \int_{z_{t4}}^{z_{t1}} \frac{dx_r dx_t dz_t}{\sqrt{(x_r - x_t)^2 + z_t^2 + (y_{r2} - y_{t1})^2}} \tag{10}$$

Here, $x_r \in (x_{r2}, x_{r3})$, $x_t \in (x_{t1}, x_{t4})$, $z_t \in (z_{t4}, z_{t1})$.

Moreover, $M_{AF} = M_{AH} = M_{CF} = M_{CH} = M_{ED} = M_{EB} = M_{GD} = M_{GB} = 0$. Please note that the sign "+" of mutual inductance expresses that the currents of the two conductors are in the same direction, and the sign "−" of mutual inductance expresses that the directions of the currents flowing in the two conductors are in the opposite directions.

Combining Eqs. (7)–(10), the total mutual inductance M between two conductors can be obtained. For example, the currents of two coils are in the same direction shown in Fig. 6(a), and the total mutual inductance M can be expressed as: $M = M_{AE} + M_{CG} - M_{AG} - M_{CE} + M_{BH} + M_{DF} - M_{BF} - M_{DH}$.

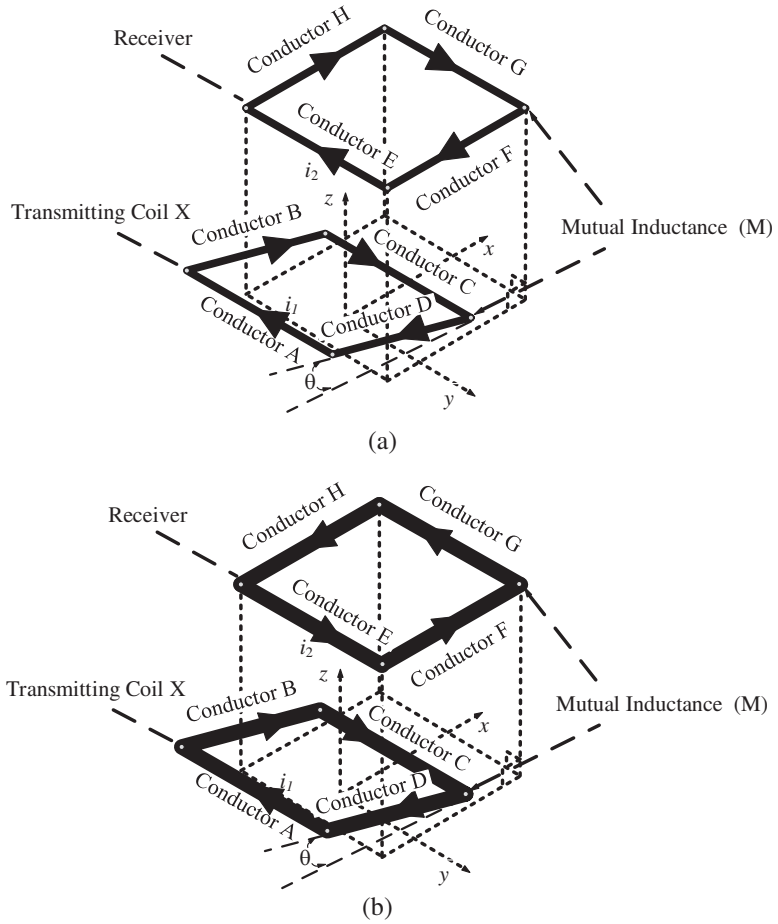

Figure 6. The relationship of current of two wire.

The directions of the currents of two coils are different are shown in Fig. 6(b), and the total mutual inductance M can be expressed as: $M = -M_{AE} - M_{CG} + M_{AG} + M_{CE} - M_{BH} - M_{DF} + M_{BF} + M_{DH}$.

The total mutual inductance M highly depends on the positions of transmitter and receiver. The position influences the total mutual M by the magnetic fields generated by transmitter and receiver.

3.3. Magnetic Flux Density Analysis in 3D Cross Coil Structure

Assume that a unit vector from a point on transmitter $p_1(x_1, y_1, z_1)$ to an arbitrary point $p(x, y, z)$ is $\widehat{r_1}$, and a unit vector from a point on receiver $p_2(x_2, y_2, z_2)$ to $p(x, y, z)$ is $\widehat{r_2}$, $\widehat{r_1}$ and $\widehat{r_2}$ which can be expressed as follows:

$$\widehat{r_1} = \frac{\overline{r_{p_1p}}}{|r_{p_1p}|} = \frac{(x - x_1)\,\widehat{x} + (y - y_1)\,\widehat{y} + (z - z_1)\,\widehat{z}}{\sqrt{(x - x_1)^2 + (y - y_1)^2 + (z - z_1)^2}} \tag{11}$$

$$\widehat{r_2} = \frac{\overline{r_{p_2p}}}{|r_{p_2p}|} = \frac{(x-x_2)\,\widehat{x} + (y-y_2)\,\widehat{y} + (z-z_2)\,\widehat{z}}{\sqrt{(x-x_2)^2 + (y-y_2)^2 + (z-z_2)^2}} \tag{12}$$

In practice, current $i_T(t)$ power-on transmitter is expressed as $i_T(t) = I_m \cos(\omega t + \theta_T)$. Assume that the direction of $i_T(t)$ agrees with Fig. 6(b). The magnetic flux density (B-field) induced by transmitter at an arbitrary point $p(x, y, z)$ can be expressed as

$$\begin{aligned}\overline{\mathbf{B}_{Tran}} &= \frac{u_0 I_m \cos(\omega t + \theta_T)}{4\pi} \oint \frac{\overline{dl} \times ((x-x_1)\,\widehat{x} + (y-y_1)\,\widehat{y} + (z-z_1)\,\widehat{z})}{\left((x-x_1)^2 + (y-y_1)^2 + (z-z_1)^2\right)^{3/2}} \\ &= \frac{u_0 I_m \cos(\omega t + \theta_T)}{4\pi} \left\{ \begin{array}{c} \int_A \frac{1}{r_1^3} \left[\begin{array}{l} \widehat{x}\,(z-z_1)\,dy \\ -\widehat{z}\,(x-x_1)\,dy \end{array} \right] \\ + \int_B \frac{1}{r_1^3} \left[\begin{array}{l} \widehat{x}\,(y_1-y)\,dz + \\ \widehat{y} \left(\begin{array}{l} (x-x_1)\,dz \\ -(z-z_1)\,dx \end{array} \right) \\ + \widehat{z}\,(y-y_1)\,dx \end{array} \right] \\ + \int_C \frac{1}{r_1^3} \left[\begin{array}{l} \widehat{x}\,(z-z_1)\,dy \\ -\widehat{z}\,(x-x_1)\,dy \end{array} \right] \\ + \int_D \frac{1}{r_1^3} \left[\begin{array}{l} \widehat{x}\,(y_1-y)\,dz \\ + \widehat{y} \left(\begin{array}{l} (x-x_1)\,dz \\ -(z-z_1)\,dx \end{array} \right) \\ + \widehat{z}\,(y-y_1)\,dx \end{array} \right] \end{array} \right\} \end{aligned} \tag{13}$$

$\overline{\mathbf{B}_{Tran}}$ has three components, $\mathbf{B}_x$, $\mathbf{B}_y$, and $\mathbf{B}_z$, which can be written as follows:

$$\mathbf{B}_x|_{Tran} = \frac{\mu_0 I_m \cos(\omega t + \theta_T)}{4\pi} \left\{ \begin{array}{l} \int_A \frac{1}{r_1^3} \widehat{x}\,(z-z_1)\,dy \\ + \int_B \frac{1}{r_1^3} \widehat{x}\,(y_1-y)\,dz \\ + \int_C \frac{1}{r_1^3} \widehat{x}\,(z-z_1)\,dy \\ + \int_D \frac{1}{r_1^3} \widehat{x}\,(y_1-y)\,dz \end{array} \right\} \tag{14}$$

$$\mathbf{B}_y|_{Tran} = \frac{\mu_0 I_m \cos(\omega t + \theta_T)}{4\pi} \left\{ \begin{array}{l} \int_B \frac{1}{r_1^3} \widehat{y} \left(\begin{array}{l} (x-x_1)\,dz \\ +(z-z_1)\,dx \end{array} \right) \\ vspace1mm \; + \int_D \frac{1}{r_1^3} \widehat{y} \left(\begin{array}{l} (x-x_1)\,dz \\ +(z-z_1)\,dx \end{array} \right) \end{array} \right\} \tag{15}$$

$$\mathbf{B}_z|_{Tran} = \frac{\mu_0 I_m \cos(\omega t + \theta_T)}{4\pi} \left\{ \begin{array}{l} \int_A \frac{1}{r_1^3} \widehat{z}\,(x_1-x)\,dy \\ + \int_B \frac{1}{r_1^3} \widehat{z}\,(y-y_1)\,dx \\ + \int_C \frac{1}{r_1^3} \widehat{z}\,(x_1-x)\,dy \\ + \int_D \frac{1}{r_1^3} \widehat{z}\,(y-y_1)\,dx \end{array} \right\} \tag{16}$$

For simplicity, assume that the receiver is parallel to xy-plane, and the angle of transmitter and receiver is θ_{TR} as shown in Fig. 7. θ_{TR} is a space angle, and the weights of $\mathbf{B}_x|_{Tran}$, $\mathbf{B}_y|_{Tran}$, and

$\mathbf{B}_z|_{Tran}$ in the direction of coil axis are

$$\begin{cases} \mathbf{B}_x|_{TranLR} = 0 \\ \mathbf{B}_y|_{TranLR} = 0 \\ \mathbf{B}_z|_{TranLR} = B_z|_{Tran}\cos(\theta_{TR}) \end{cases} \tag{17}$$

Therefore, only $\mathbf{B}_z|_{Tran}$ can couple with the receiver, and the receiver is parallel to xy-plane. Furthermore, the magnetic flux generated by transmitter in the area of receiver is

$$\Phi = \int_S \overline{\mathbf{B}_{Tran}} \bullet dS = \int_{S_1} \mathbf{B}_z|_{TranLR} \bullet d\mathbf{S} \tag{18}$$

where S_1 is the weight of receiving coil area in the direction of z-axis.

The mutual inductance M of transmitter and receiver can be expressed

$$M = \frac{N_1 N_2 \Phi}{I_m \cos(\omega t + \theta_T)} \tag{19}$$

where N_1 is the turn number of transmitter coil, and N_2 is the turn number of receiver.

Combining Eqs. (17) and (18), the mutual inductance M is

$$M = \frac{N_1 N_2 \left[\int_{S_2} \mathbf{B}_z|_{Tran}\cos(\theta_{TR}) \bullet d\mathbf{S}\right]}{I_m \cos(\omega t + \theta_T)} \tag{20}$$

Considering Eq. (2) the efficiency is a function of θ_{TR}

$$\eta = \frac{\omega_0^2 [M(\theta_{TR})]^2 R_L}{(R_P + r_1)(R_L + r_2)^2 + \omega_0^2 [M(\theta_{TR})]^2 (R_L + r_2)} \tag{21}$$

Based on Eq. (21), the best θ_{TR} can be calculated with the principle of maximum efficiency, and the best θ_{TR} is marked as θ_{TRM} in this thesis.

4. NUMERICAL SIMULATION OF 3D CROSS COIL STRUCTURE

In this part, the numerical simulation of 3D crossed coil technique will be presented. The purpose of the numerical simulation is verifying the mathematical model of 3D crossed coil technique shown in Section 3. As shown in Fig. 7, the transmission coils with different θ_{TR} are included in transmitter which are included in transmitter. Only one transmission coil has power-on current. In practice, the system controller will choose the transmitter coil with space angle θ_{TR}, which is closest to θ_{TRM}.

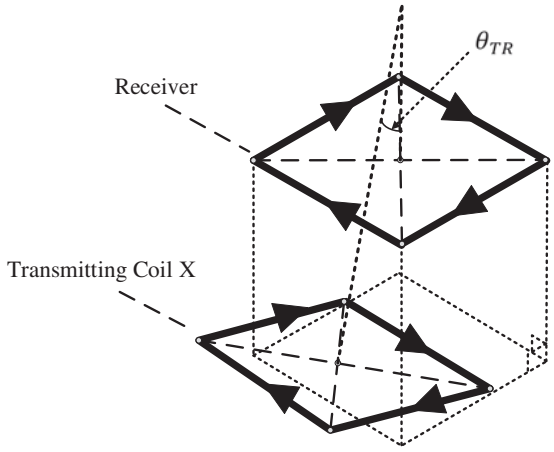

Figure 7. Diagram of angle of transmitter and receiver.

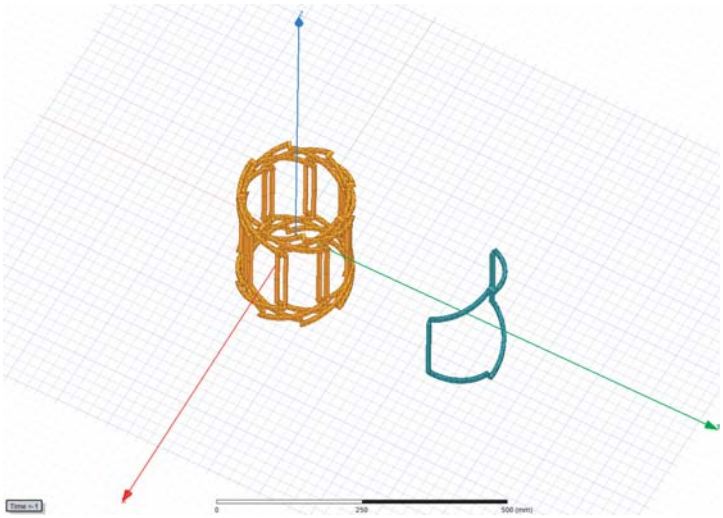

Figure 8. Diagram of the numerical simulation model of 3D cross coil.

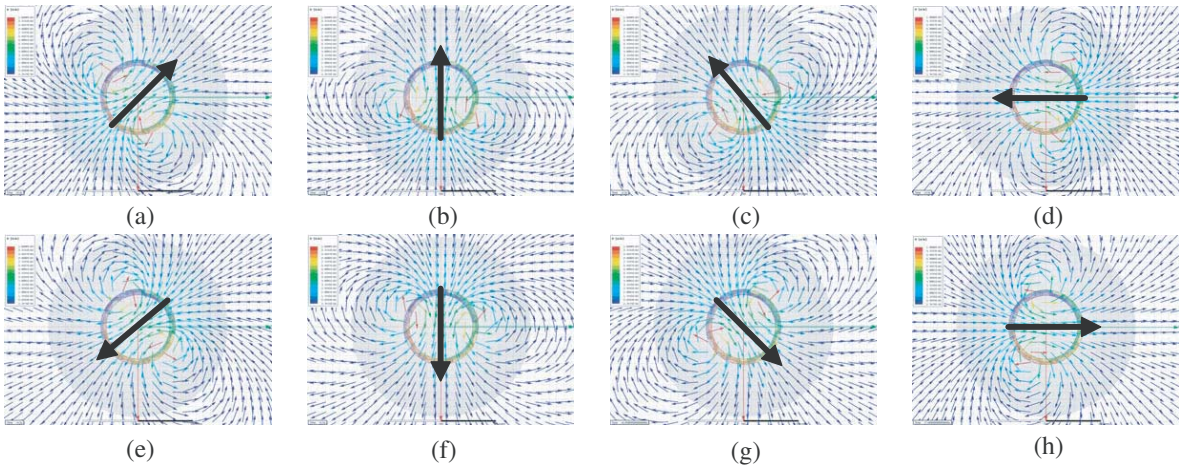

Figure 9. Diagram of the magnetic field with different direction.

Based on the mathematical model, the WPT system with a 3D cross coil structure simulation model is built as shown in Fig. 8, and the magnetic field will be calculated by finite element method (FEM), and the mutual inductance also will be gotten.

Assume that the transmitter includes eight coils. When the current passes in the transmitter turn by turn, the magnetic fields with different directions will be generated, as shown in Fig. 9.

In Fig. 9, the direction of magnetic is parallel to the surface normal vector $\overrightarrow{n}$ of transmitter coil. Furthermore, maximum energy transfer efficiency can be achieved when the surface normal vector $\overrightarrow{n}$ of the receiver coil and the direction of magnetic are parallel. As shown in Fig. 9, the direction of the magnetic field is an important factor determining energy transfer efficiency. By exploiting the fact that the direction of the magnetic field can be controlled by changing the space angle θ_{TR} of transmitting coils, the energy can be transmitted on particular position. If the position of receiver can be confirmed, the best θ_{TR}, which can achieve a high efficiency, can be calculated.

The position of receiver is related directly to the mutual inductance M between receiver and each transmitter coil. In this paper, the position of receiver is assumed as shown in Fig. 9, and the mutual inductance M can be calculated by Ansoft Maxwell in Table 1.

The value of mutual inductance in Table 1 is different obviously. Furthermore, the maximum M in Table 1 is the mutual inductance between receiver and Coil 4 in transmitter. The energy could be

Table 1. The mutual inductance between receiver and transmitter coil.

	Coil 1	Coil 2	Coil 3	Coil 4	Coil 5	Coil 6	Coil 7	Coil 8
M (μH)	1.29	0.73	1.46	3.04	2.66	0.56	0.87	1.18

transferred efficiently by Coil 4. If the energy received by the receiver is satisfactory, Coil 4 will be used for transmitter coil. However, the most common case is the energy that receiver received is not satisfactory. In practice, the transmitter could be adjusted slightly, such as rotating the transmitter slightly by machines. The adjustment will help the system achieve better performance, and the system will be more efficient. In addition, there may be a case that two mutual inductances are close, and the method dealing with this case adjusts the transmitter substantially, which makes a difference obviously in Table 1.

Assuming that Coil 4 is used for transmitter coil after the adjustment. The resonance frequency should be chosen based on the actual demand. In this paper, the resonance frequency is 1 MHz. The value of capacitance used for resonance circuit can be calculated:

$$\omega L_{TR} = \frac{1}{\omega C_{TR}} \tag{22}$$

where ω is the resonance frequency of resonance circuit, L_{TR} the inductance value of transmitter coil (Coil 4), and C_{TR} the value of capacitance using for resonance circuit.

When the circuit parameters have been calculated, the field-circuit coupled simulation model will be built by Ansoft Maxwell. The results of the field-circuit coupled FEM simulation model are shown in Fig. 10. The field-circuit coupled FEM simulation model indicates that the mathematical model meets the expectation satisfactorily. The mathematical model is also verified initially by the field-circuit coupled FEM simulation model.

In Fig. 10, the energy is transferred satisfactorily from transmitter to the receiver. The magnetic field intensity vector is calculated, and one of time step results is chosen shown in Fig. 10(a). The magnetic field intensity vector generated by transmitter and receiver is clearly shown in Fig. 10(a). In Fig. 10(b), magnetic flux density is calculated, and the coupling field of transmitter and receiver can also be seen clearly. Because only one transmitter coil loads the current, and the other transmitter coils have been broken off, the interference of the broken coils is not obvious, and the unnecessary leakage flux is tiny. Thus, in Fig. 10, the energy is transferred efficiently in the specific direction in which the receiver coil is located.

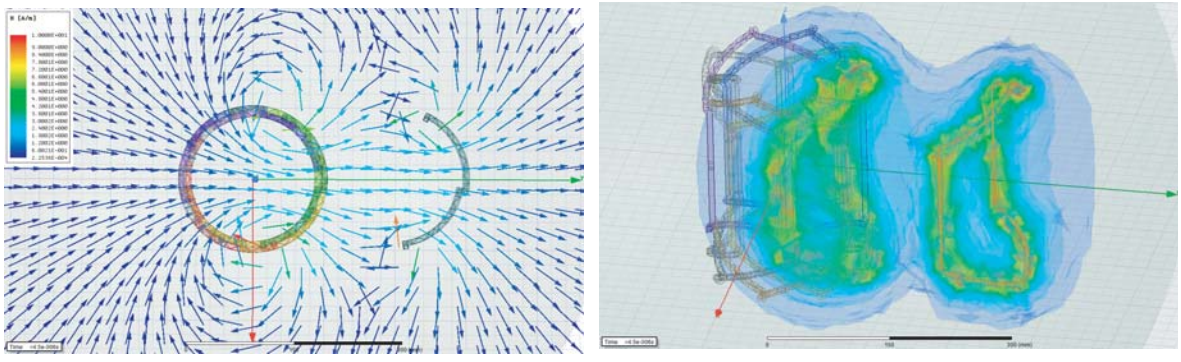

(a) (b)

Figure 10. The results of the field-circuit coupled simulation.

5. EXPERIMENT VERIFICATION

In this section, the experiment verification is done, and in the experiment, the WPT hardware system with the proposed coil structure is built. The experiment results are also compared with the simulation

ones. Our results show that the novel coil structure has a better performance in misalignment situation than the traditional system.

Based on the theoretical analysis presented in the previous sections, the implemented WPT system block diagram is shown in Fig. 11, which is composed of two parts. One part is a transmitter including a power generator and selecting transmitter coil system, and the other is a receiver with resistive load. As explained in Section 3, the transmitter coil should be selected with the largest mutual inductance to achieve a better system performance. The detailed explanation of the experiment is provided in the next part.

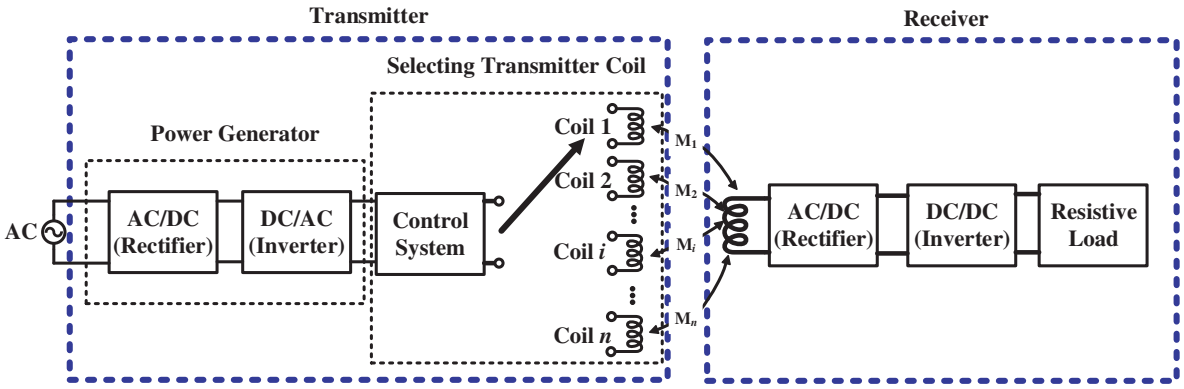

Figure 11. The diagram of the simulation model of capacitance of the insulating layer.

5.1. 3D Cross Coil Structure in the Transmitter

Figure 11 shows the mentioned 3D cross coil structure block diagram. In Fig. 11, the power generator is composed of an AC/DC Rectifier and a DC/AC Inverter. The detailed hardware architecture of the transmitter is shown in Fig. 13. The AC/DC rectifier converts 50 Hz commercial alternating current to direct current. The DC/AC Inverter converts direct current to 1 MHz alternating current. The power generator has an input AC voltage. The output voltage V_{DC} is applied to the DC/AC inverter composed of power MOSFET. The main roles of the power generator are to control the system frequency and transferred power. Moreover, the direction of the magnetic field can be controlled by modifying the space angle of transmitter coil. And the magnitude of the magnetic field can be controlled by the amplitude of the current output in the power generator shown in Fig. 11. The control system will recognize the transmitter coil used for transfer power to the receiver. Receiver in Fig. 11 is composed of a receiving coil, an AC/DC converter, and a resistance load. The parameters of the receiver are shown in Table 2.

In this paper, the size of the transmitter coil is 120 mm × 100 mm shown in Fig. 11. The quality factor Q of the transmitter coil is

$$Q = \frac{\omega L}{r} \tag{23}$$

Here, ω is the frequency of the resonance circuit. L is the inductance of transmitter coil. r is the resistance of transmitter coil.

A better system performance needs a high level of Q [10]. When the frequency of the resonance circuit is fixed, the quality factor Q will increase with the increasing value of $\frac{L}{r}$. In order to increase transmission power, we should increase the inductance of transmitter coil and decrease the resistance of transmitter coil. Thus, the transmitter coil structure with several turns (shown in Fig. 12) is adopted in the WPT system. Moreover, all the transmitter coils have the same design scheme.

The detailed parameters of the implemented coil structure are shown in Table 2. To create a resonance of 1 MHz, L and C of transmitter and receiver are satisfied with $\omega L = \frac{1}{\omega C}$. In order to minimize the resistance (R), 2 mm 2 mm Litz coils are used.

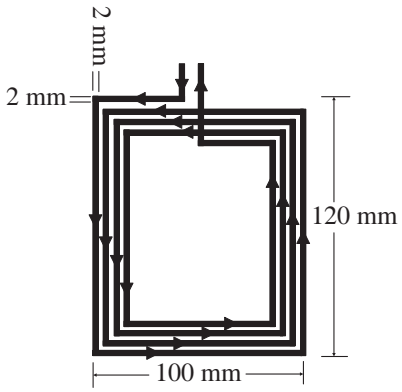

Figure 12. Diagram of the transmitter coil structure.

Table 2. The detail parameters of the implemented coil structure.

Parameters	Frequency [MHz]	L (μH)	C (pF)	Width [mm]	Height [mm]	Turns	Thickness [mm]
Coil 1	2.33	7.76	800	120	100	5	4
Coil 2	2.33	7.76	800	120	100	5	4
Coil 3	2.33	7.76	800	120	100	5	4
Coil 4	2.33	7.76	800	120	100	5	4
Coil 5	2.33	7.76	800	120	100	5	4
Receiver Coil	2.33	8.28	748	125	105	5	4

5.2. 3D Crossed Coil Structure WPT System Hardware Design

In Fig. 13, the rectifier diodes are silicon controlled rectifiers, and the voltage V_{DC} can be controlled by changing the duration of the gate plus signals of the silicon controlled rectifiers. The transfer frequency in Fig. 13 can be controlled by the plus signal of the N-Channel MOSFET. Measurement oscilloscope is from Agilent company, and inverter power supply is built by ourselves. The detailed parameters of the implemented coil structure are shown in Table 2.

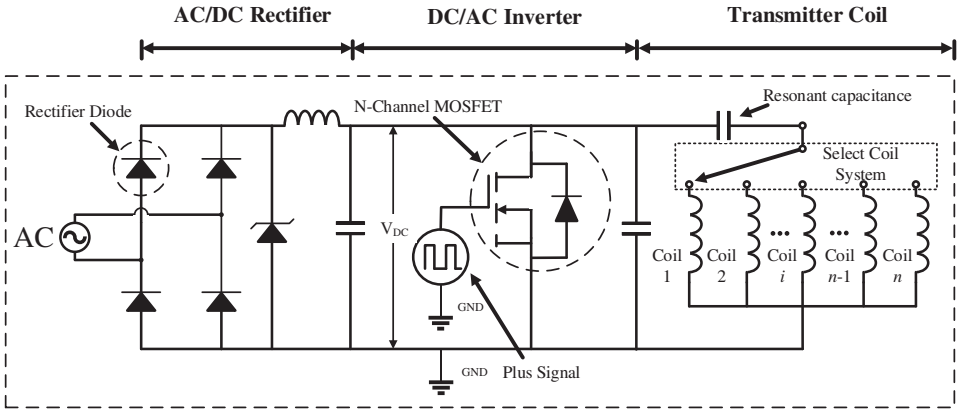

Figure 13. The detailed hardware architecture of the transmitter.

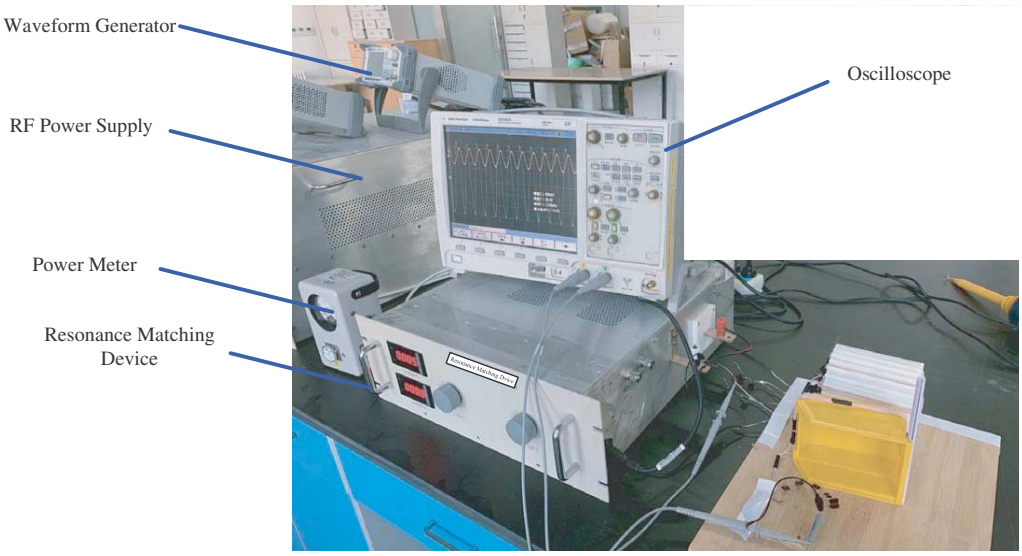

(a) The diagram of the experimental system

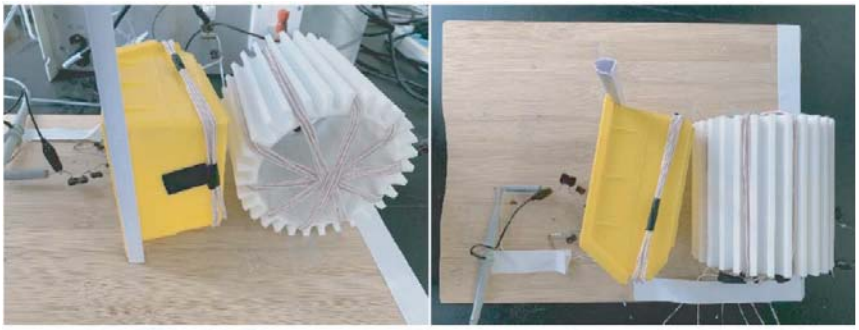

(b) The diagram of the experimental coil structure

Figure 14. Experiment verification of 3D Cross Coil Structure WPT System.

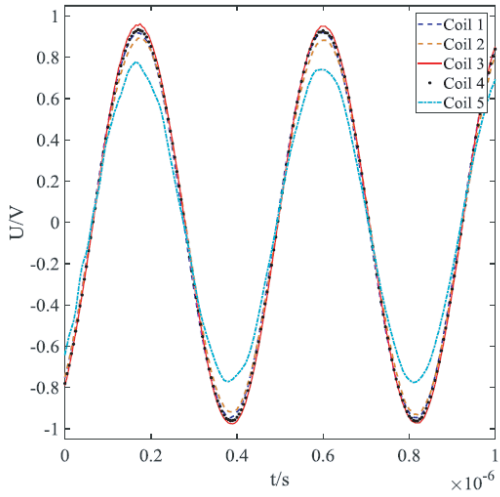

Figure 15. The load voltage when the transmitter coil load power respectively.

5.3. Experimental Results

We use resistance load to demonstrate that the 3D cross coil structure WPT system can transfer the power to the misalignment receiver. An oscilloscope which shows the real-time load voltage is used to indicate the transfer status. Fig. 14 shows pictures of experiment verification of the 3D cross coil structure WPT system, and in Fig. 14, there are 5 transmitter coils which are included in the transmitter. Fig. 15 shows the load voltage of the resistance load when the transmitter coil powers on, respectively. In the experimental verification, in Fig. 15, transmitter Coil 3 has the maximum mutual inductance with the misaligned receiver, thus the transfer power is maximum. Transmitter Coil 1 and transmitter Coil 4 also have high transfer power in Fig. 15, and the reason is likely that the mutual inductance between the transmitter Coil 1, Coil 4, Coil 3 and misaligned receiver has small difference. The efficiency of the system is 86.7%. We can see that the 3D cross coil structure can also transfer power to the misaligned receiver with no alignment and orientation requirement.

6. CONCLUSION

In this work, we demonstrate that the 3D crossed coil structure can be used in a misaligned wireless power transfer system. In the theory model, the magnetic field equation of different relationships between transmitter and receiver is deducted, and the efficiency η is a function about that the transmitter coil spatial angle θ_{TR} has been proved. In simulation model, we get the conclusion: the suitable spatial angle θ_{TR} can help get a higher efficiency η, and the conclusion has been verified. The closer the transmitter is to the coaxiality, the higher the efficiency will be obtained. In the experiment part, the verified experiment is also done, and the efficiency of the system is 86.7%. The simulated and experimental results show that the new three-dimensional coil structure has a better performance in the misalignment situation than the plane coil structure in the misaligned wireless power transfer system. Compared to the theory model, the simulation model shows that in the case of the maximum mutual inductance M between transmitter cell coil and receiver, the maximum efficiency will be achieved. Compared to the simulation part, the experiment shows that the transmitter coils with different space angles have different efficiencies; however, the difference of efficiency is smaller than the simulation part. Rotating magnetic field generation and 3D crossed coil structure are also demonstrated to keep the system working in a reliable and optimum working status. Future work will focus on increasing the system efficiency when multiple loads are applied, and we will also focus on the precise control of the 3D crossed coil system, because the precise control of the 3D crossed coil system is also important for the system.

ACKNOWLEDGMENT

This research was supported by the National Natural Science Foundation of China under Grant No. 51677177.

REFERENCES

1. Kurs, A., A. Karalis, R. Moffatt, J. D. Joannopoulos, P. Fisher, and M. Soljacic, "Wireless power transfer via strongly coupled magnetic resonances," *Science*, Vol. 317, No. 5834, 83–86, 2007.
2. Mou, X., D. T. Gladwin, R. Zhao, and H. Sun, "Survey on magnetic resonant coupling wireless power transfer technology for electric vehicle charging," *IET Power Electronics*, Vol. 12, No. 12, 3005–3020, Oct. 16, 2019.
3. Kim, Y. and S. Lim, "Compact magnetic coupled resonator with high efficiency during misaligned wireless power transmission," *Journal of Electromagnetic Waves and Applications*, Vol. 27, No. 15, 1942–1948, Oct. 1, 2013.
4. Lee, K. and D.-H. Cho, "Diversity analysis of multiple transmitters in wireless power transfer system," *IEEE Transactions on Magnetics*, Vol. 49, Nos. 6, 2, 2946–2952, Jun. 2013.
5. Wu, D., Q. Sun, X. Wang, and T. He, "Analytical calculation of mutual coupling between two misaligned rectangular coils with rectangular cross-section in wireless power applications," *Journal of Physics D — Applied Physics*, Vol. 50, No. 43, 43LT06, Nov. 1, 2017.

6. Zhang, W., T. Zhang, Q. Guo, L. Shao, N. Zhang, X. Jin, and J. Yang, "High-efficiency wireless power transfer system for 3D, unstationary free-positioning and multi-object charging," *IET Electric Power Applications*, Vol. 12, No. 5, 658–665, May 2018.
7. Tan, P., L. Ye, S. Cao, and B. Zhang, "Design and implement an adaptive position adjustment coupler for coil-misaligned inductive contactless power transfer system," *2017 IEEE Applied Power Electronics Conference and Exposition (APEC)*, 1590–1593, Tampa, FL, 2017.
8. Jonah, O., S. V. Georgakopoulos, and M. M. Tentzeris, "Orientation insensitive power transfer by magnetic resonance for mobile devices," *2013 IEEE Wireless Power Transfer (WPT)*, 5–8, Perugia, 2013.
9. Wang, Y., J. Kang, W. Li, and Q, Wang, "Three dimensional rotatable omnidirectional MCR WPT systems," *IET Power Electronics*, Vol. 13, No. 2, 256–265, 2020.
10. Seo, D.-G., S.-H. Ahn, J.-H. Kim, W.-S. Lee, S.-T. Khang, S.-C. Chae, and J.-W. Yu, "Power transfer efficiency for distance-adaptive wireless power transfer system," *2018 International Applied Computational Electromagnetics Society Symposium (ACES)*, 1–2, Denver, CO, Mar. 25–29, 2018.
11. Tan, S. Y., H. J. Lee, K. Y. Lau, and P. J. Ker, "Simulation of 4-coils magnetic resonance coupling for multiple receivers wireless power transfer at various transmission distance," *2018 IEEE Student Conference on Research and Development (SCOReD)*, 1–5, Selangor, Malaysia, Nov. 26–28, 2018.
12. Ng, W. M., C. Zhang, D. Lin, and S. Y. Ron Hui, "Two- and three-dimensional omnidirectional wireless power transfer," *IEEE Transactions on Power Electronics*, Vol. 29, No. 9, 4470–4474, 2014.
13. Kawasaki, S., Y. Kobayashi, and S. Yoshida, "High-power, high-efficiency microwave circuits and modules for wireless power transfer based on green-eco technology," *2013 IEEE Radio and Wireless Symposium*, 28–30, Austin, TX, Jan. 20–23, 2013.
14. Schafer, S., M. Coffey, and Z. Popovic, "X-band wireless power transfer with two-stage high-efficiency GaN PA/rectifier," *2015 IEEE Wireless Power Transfer Conference (WPTC)*, 1–3, Boulder, CO, May 13–15, 2015.
15. Zhang, Y., Z. Zhao, and K. Chen, "Frequency decrease analysis of resonant wireless power transfer," *IEEE Transactions on Power Electronics*, Vol. 29, No. 3, 1058–1063, Mar. 2014.
16. Ye, Z., Y. Sun, X. Liu, P. Wang, C. Tang, and H. Tian, "Power transfer efficiency analysis for omnidirectional wireless power transfer system using three-phase-shifted drive," *Energies*, Vol. 11, No. 8, 2159, Aug. 2018.
17. Zhao, C., Z. Wang, J. Du, J. Wu, S. Zong, and X. He, "Active resonance wireless power transfer system using phase shift control strategy," *2014 IEEE Applied Power Electronics Conference and Exposition — APEC 2014*, 1336–1341, Fort Worth, TX, Mar. 16–20, 2014.
18. Sandoval, F. S., S. M. Torres Delgado, A. Moazenzadeh, and U. Wallrabe, "A 2-D magnetoinductive wave device for freer wireless power transfer," *IEEE Transactions on Power Electronics*, Vol. 34, No. 11, 10433–10445, Nov. 2019.
19. Mohammad, M., E. T. Wodajo, S. Choi, and M. E. Elbuluk, "Modeling and design of passive shield to limit EMF emission and to minimize shield loss in unipolar wireless charging system for EV," *IEEE Transactions on Power Electronics*, Vol. 34, No. 12, 12235–12245, Dec. 2019.
20. Machura, P. and Q. Li, "A critical review on wireless charging for electric vehicles," *Renewable & Sustainable Energy Reviews*, Vol. 104, 209–234, Apr. 2019.
21. Trivino-Cabrera, A. and J. A. Aguado Sanchez, "A review on the fundamentals and practical implementation details of strongly coupled magnetic resonant technology for wireless power transfer," *Energies*, Vol. 11, No. 10, Oct. 2018.
22. Yan, Z., Y. Li, C. Zhang, and Q. Yang, "Influence factors analysis and improvement method on efficiency of wireless power transfer via coupled magnetic resonance," *IEEE Transactions on Magnetics*, Vol. 50, No. 4, 1–4, Art No. 4004204, 2014.
23. Abatti, P. J., C. M. de Miranda, M. A. P. da Silva, and S. F. Pichorim, "Analysis and optimisation of three-coil wireless power transfer systems," *IET Power Electronics*, Vol. 11, No. 1, 68–72, Jan. 12, 2018.